

Article

The Eccentric Compression Performance of Spirally Stiffened Thin-Walled Square Concrete-Filled Steel Tubular Laminated Composite Members

Zhenshan Wang ^{1,2,*}, Yanan Su ², Jun Wei ³, Junlong Lu ² and Xiaolei Li ²

¹ State Key Laboratory of Northwest Arid Ecological Water Conservancy Engineering, Xi'an University of Technology, Xi'an 710048, China

² School of Civil Engineering and Architecture, Xi'an University of Technology, Xi'an 710048, China; 2200721106@stu.xaut.edu.cn (Y.S.); lujunlong@xaut.edu.cn (J.L.); lx1_832277@163.com (X.L.)

³ School of Civil Engineering, Suzhou University of Science and Technology, Suzhou 215009, China; Qjweijun@163.com

* Correspondence: wangzhenshan@xaut.edu.cn

Abstract: To enhance the local buckling resistance of thin-walled steel pipes and enhance their fire and corrosion resistance, a new spirally stiffened thin-walled square concrete-filled steel tubular laminated composite member with transverse ribs is proposed. Through the four forms of combined members for eccentric pressure testing, it was found that: ordinary thin-walled steel pipe concrete drum buckling is more severe; with spiral ribs, the buckling is limited between the stiffening ribs; and the deformation is significantly reduced. By addressing the problem of cooperative work between the inner and outer structural layers of new components, it was found that, after setting constraints such as steel bars, the integrity of the two can be ensured, and the stress performance is significantly improved; compared to ordinary steel pipe concrete, the load-carrying capacity is 17.9% higher, and the deformation capacity is roughly equivalent. Spiral ribs as a new form of spatial restraint, in addition to increasing the local bending stiffness, manifest an overall restraint role in limiting lateral deformation of the steel pipe, whereas the role of vertical stiffness is insignificant. Based on test evidence, the influences of the width to thickness ratio of spiral ribs and pitch were determined, and reasonable structural measures for the members were given. Through the N–M relationship curve, the limit of damage in compression and tension under eccentricity was obtained at an eccentricity of about 0.9. Finally, a method for calculating the eccentric compressive ultimate load capacity of this new composite member was proposed.

Keywords: thin-walled steel pipe concrete; spirally stiffened ribs; eccentric pressure; ultimate load-carrying capacity; numerical simulation



Citation: Wang, Z.; Su, Y.; Wei, J.; Lu, J.; Li, X. The Eccentric Compression Performance of Spirally Stiffened Thin-Walled Square Concrete-Filled Steel Tubular Laminated Composite Members. *Buildings* **2022**, *12*, 1151. <https://doi.org/10.3390/buildings12081151>

Academic Editor: Francisco López Almansa

Received: 9 July 2022

Accepted: 28 July 2022

Published: 3 August 2022

Publisher's Note: MDPI stays neutral with regard to jurisdictional claims in published maps and institutional affiliations.



Copyright: © 2022 by the authors. Licensee MDPI, Basel, Switzerland. This article is an open access article distributed under the terms and conditions of the Creative Commons Attribution (CC BY) license (<https://creativecommons.org/licenses/by/4.0/>).

1. Introduction

The use of rectangular concrete-filled steel tubes is relatively widespread in high-rise buildings and bridge structures due to its advantages of a simple structure and high flexural rigidity. The restraint of the rectangular section of a steel pipe is mainly concentrated in the corners, and the restraint effect of the straight side is greatly reduced. It is important to assess the beneficial effects of the rectangular cross-section concrete-filled steel tube hoops. To reduce the amount of steel used for components and improve their cost-effectiveness, some researchers proposed thin-walled concrete-filled steel tubes. By addressing the local buckling problem of thin-walled steel pipes, plate stiffeners are often added in engineering. Scholars studied the use of longitudinal stiffening ribs for steel pipe concrete members and found that the stiffening ribs can strengthen the steel pipe restraint support, reduce bulging deformation, enhance the interaction between the core concrete and the pipe wall, and thus retard the local buckling of the member [1–3].

In order to limit the transverse deformation of a steel pipe and improve the hoop effect, many scholars have studied continuous diagonal stiffening ribs [4–7] and found that diagonal ribs can improve the composite effect and limit the local buckling of steel pipes with higher material performance utilization. However, when the span of the components is large, the larger the stiffener spacing is, the lower the local stability of the component is, without changing the number of inclined ribs and its inclination angle, resulting in poor overall performance of the component. Therefore, the use of inclined rib constraints requires flexible control of inclination. To improve the integrity of stiffening ribs and concrete, scholars conducted experimental research on perforated steel plate stiffeners [8–11] and found that the perforated rib specimen showed a high ductility, which could improve the local stability of the external steel pipe and increase the longitudinal stress of the core concrete. It is suggested that the opening spacing of the stiffened rib of the perforated steel plate should be twice the diameter of the opening to better exert its ductility and energy dissipation capacity.

For thin-walled steel pipe concrete members, facing the problem of rapid degradation of the force performance, some scholars used the setting of the spiral hoop and ring hoop and other forms to improve the deformation capacity [12–15]. They found that the setting of the spiral hoop can improve the non-uniform restraint of the square steel pipe, delaying the onset of local buckling of the rectangular steel pipe, and the restraint is stronger than the vertical plate stiffening ribs. Wu et al. [16] studied the compressive performance of a composite thin-walled circular section steel pipe column concrete with hoop reinforcement and found that the hoop reinforcement significantly improved the load-carrying capacity and ductility of the column. The seismic energy dissipation capacity of the spiral stirrup column led scholars to conduct low-frequency cyclic reciprocating load tests [17–19]. The results show that the spiral stirrup can improve the deformation capacity and the flexural bearing capacity of the column. In order to further enhance the lateral restraint effect of steel tubes, many scholars conducted experimental studies on concrete-filled steel tubular members with tie rods and tie plates [20–22] and found that reducing the tie rod spacing and installing tie plates can improve the working performance of the columns and increase the bearing capacity and deformation capacity of the specimens. In addition, the setting of restraint rods can make the restraint effect of the steel pipe wall on the core concrete more uniform, change the local buckling deformation state of the steel pipe, and significantly improve the axial compressive bearing capacity and ductility of the square steel tube concrete column.

For thin-walled steel pipe concrete columns, the influence of the diameter to thickness ratio was examined [23–27], the larger the diameter to thickness ratio, the more severe the local buckling of the column, and the location of its onset is closer to the end of the column, that is, the strength of the column decreases with the increase in the diameter to thickness ratio. On this basis, some scholars proposed the use of an oversized diameter to thickness ratio combined with columns. Wang [28], Zhou [29], Child [30], and Ci [31] conducted experimental studies and found that an oversized diameter to thickness ratio steel pipes with concrete columns with appropriately increased axial pressure ratios can increase the ductility, lateral stiffness, and energy dissipation capacity of the specimens, but the overall deformation capacity decreases. Therefore, it is of great engineering significance to delay the local buckling of ultra-large diameter–thickness ratio concrete-filled steel tubular members and improve the deformation capacity of components by structural measures. In addition, many scholars have studied the corrugated concrete-filled steel tubular members with transverse ribs [32,33]. It was found that the corrugated steel tube bears almost no axial load, and the bearing capacity of the member mainly arises from the core concrete.

In order to improve the poor fire resistance and corrosion resistance of concrete-filled steel tubes and solve the issue of the degradation rate of the mechanical properties of components being too fast, scholars studied reinforced-concrete-filled steel tube composite components [34–38]. It was found that, after the reinforcement was configured in traditional concrete-filled steel tube components, the steel skeleton arranged by longitudinal

reinforcement and stirrup formed a double constraint on the core concrete to improve the mechanical properties of the components as well as the fire resistance and corrosion resistance of the structure.

Based on the research on diagonal stiffeners and spiral stirrups, this paper proposes a new type of restraint form for spiral stiffeners. In this test, the spiral ribs adopt a fixed spacing and are helically distributed along the outer wall of the steel pipe to constrain the thin-walled steel pipe from part to the whole. At the same time, the inner steel pipe is protected by external concrete to solve the problem of the poor fire resistance and corrosion resistance of the thin-walled steel pipe. In this paper, eccentric compression tests were carried out on four types of thin-walled square-filled concrete-filled steel tubular composite columns. The composite members' failure mechanisms, load–strain distribution laws, ultimate bearing capacity, and deformation capacity were analyzed. Based on the tests, the influence of the width–thickness ratio of spiral ribs, pitch, eccentricity, and other parameters on bearing capacity was analyzed and calculated. The results provide technical support for the engineering application of new composite structures.

2. Materials and Methods

2.1. Test Processing

Four thin-walled square steel tube concrete specimens with different restraint conditions were designed. The core steel tube form is shown in Figure 1; the specimen cross-section is displayed in Figure 2, and the component parameters are listed in Table 1. Q235-B grade steel was used, and its material properties are listed in Table 2. To ensure that the steel pipe and the concrete could be jointly stressed during the loading process, the end of the component was welded with an endplate, the center hole of the endplate is $D = 100$ mm, the diameter of the small hole is 40 mm, and four pouring holes reserved on the upper-end plate were used. C30 self-compacting concrete was used, and the material properties are listed in Table 3. From the material properties in Tables 2 and 3, the average value of the three test samples was taken before the beginning of the test. Spiral ribs with a total of four limbs were set on the outside of the steel pipe; the pitch was equal to the height of the column. The steel reinforcement was HRB400 grade, and the vertical plate was welded with the spiral rib; the type of hoop was HPB300, using $\phi 6@250$. Concrete was poured inside and outside the steel pipe to complete the trial forming.

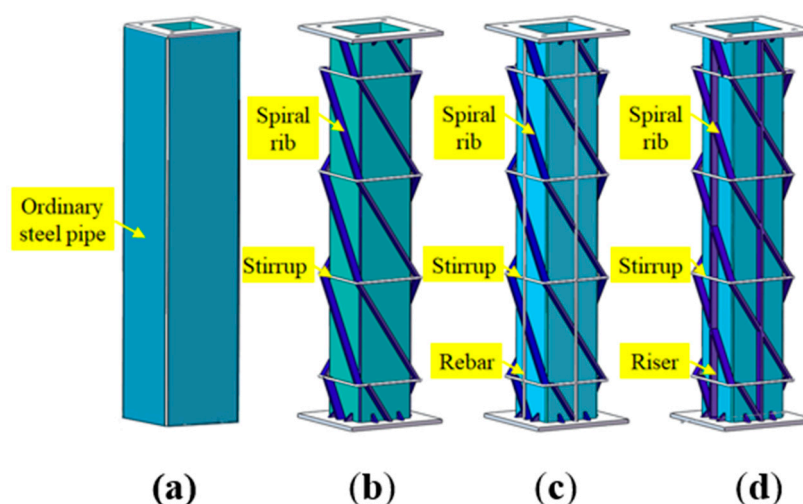


Figure 1. Core component forms. (a) Specimen 1; (b) Specimen 2; (c) Specimen 3; (d) Specimen 4.

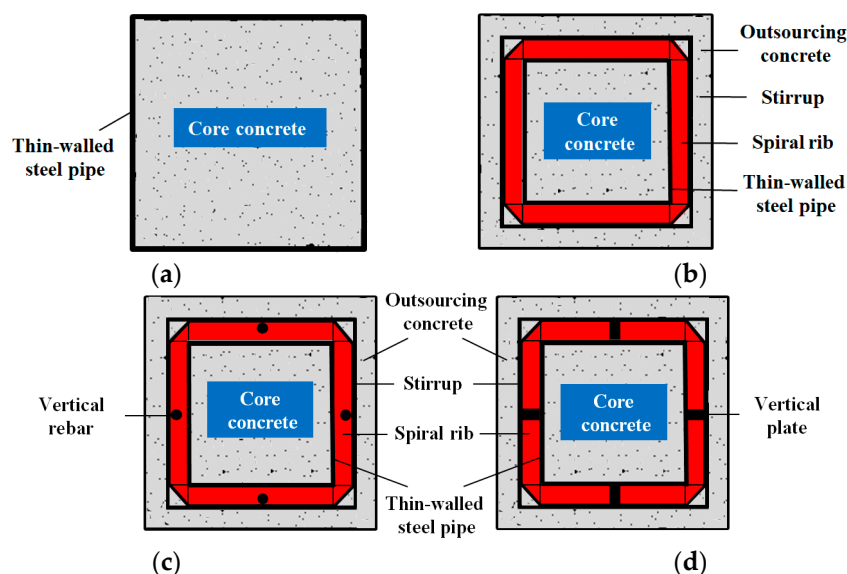


Figure 2. Cross-sectional form diagram. (a) Ordinary steel pipe; (b) Spirally ribbed steel pipe; (c) Rebar spirally ribbed steel pipe; (d) Vertical-plate spirally ribbed steel pipe.

Table 1. Specimen parameters.

| Specimen Number | Constraint Form | H/mm | d_1/mm | $d_0 \times t_0$ | $b_s \times t_s$ | $b_p \times t_p$ |
|-----------------|------------------|---------------|-----------------|------------------|------------------|------------------|
| Z1 | None | 1000 | - | 340×1 | - | - |
| Z2 | Spiral rib | 1000 | - | 220×1 | 30×3 | - |
| Z3 | Spiral rib rebar | 1000 | 14 | 220×1 | 30×3 | - |
| Z4 | Spiral rib riser | 1000 | - | 220×1 | 30×3 | 30×5 |

Table 2. Material properties of steel.

| Material | Material Property | f_y/MPa | f_u/MPa | f_y/f_u | $E_s/10^5 \text{ MPa}$ | $\delta\%$ |
|--------------------------------|-------------------|------------------|------------------|-----------|------------------------|------------|
| Steel Pipe (1.0 mm) | Q235-B | 278.70 | 388.93 | 0.72 | 2.06 | 27.3 |
| Stiffener (3.0 mm) | Q235-B | 256.94 | 363.79 | 0.71 | 2.03 | 25.7 |
| Riser (5.0 mm) | Q235-B | 252.65 | 359.26 | 0.70 | 2.02 | 22.7 |
| Rebar ($\Phi 14 \text{ mm}$) | HRB400 | 462.95 | 625.30 | 0.74 | 1.96 | 24.6 |

NOTE: δ : elongation: the ratio of the increment of gauge length to the original gauge length after tensile fracture of steel.

Table 3. Material properties of concrete.

| Concrete Strength Grade | $f_{cu,k}/\text{MPa}$ | f_{ck}/MPa | f_c/MPa | E_c/GPa |
|-------------------------|-----------------------|---------------------|------------------|------------------|
| C30 | 36.2 | 24.2 | 17.29 | 24.5 |

NOTE: $f_{cu,k}$: Standard value of compressive strength of concrete cube; f_{ck} : Standard value of axial compressive strength of concrete; f_c : Design value of axial compressive strength of concrete.

2.2. Test and Loading Scheme

The test was conducted with five displacement gauges and a percentage meter along with the column height, which was arranged in the middle of the column, the upper and lower quarters of the column length, and the bottom position, respectively. The initial eccentricity of the specimen is 0.4, and the roller support is set at the bottom. The loading device is shown in Figure 3, and the test site is shown in Figure 4. The elastic phase is controlled by the load; when the specimen enters the elastic–plastic phase, it is controlled by displacement until the load is reduced to 80% of the ultimate load and the test is completed.

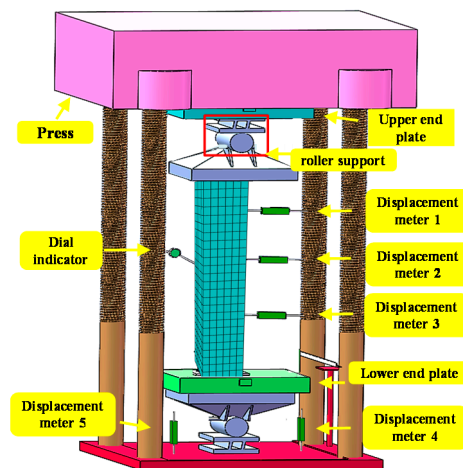


Figure 3. Test loading device.

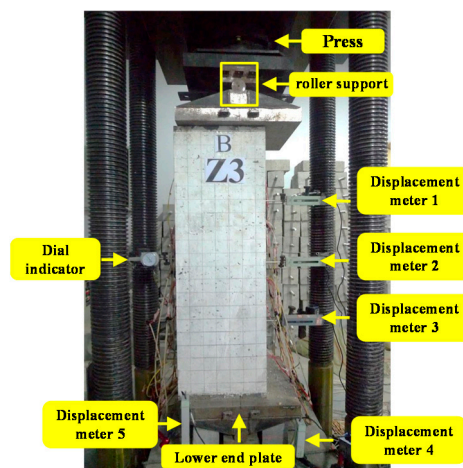


Figure 4. Test site conditions.

3. Results and Discussion

3.1. Test Procedure and Phenomena

Specimen Z1 is an ordinary thin-walled square steel tube concrete column. There was little change at the beginning of loading, and when the bias load reached 850 kN, local buckling occurred at 200 mm from the top of the column (Figure 5a). When the load increased to about 1240 kN, local buckling occurred in the middle of side D of the specimen (Figure 5b). When the load reached 1775 kN, the deformation of the previously buckled tubes increased, and the specimen reached the ultimate load-carrying capacity. Thereafter, the load started to drop and reached 1600 kN when several corrugated zones indicative of local flexural deformation appeared on the compressed side of the specimen on the A-side (Figure 5c). The test was then stopped.

Specimen Z2 is a spiral rib-reinforced thin-walled concrete-filled steel tubular laminated column, and no obvious deformation occurred at the onset of loading. When the load reached 780 kN, cracks appeared on the compressed side of specimen B, accompanied by a brittle cracking sound (Figure 6a). When loaded to 1700 kN, several transverse cracks appeared on the external concrete of the tensioned surface (Figure 6b); as the loading continued, the transverse cracks on the tensioned face widened and the concrete on the compressed face appeared to be spalling (Figure 6c). At the end of the test, the external concrete spalled and the middle and upper part of the compressed surface, as well as the lateral steel tube, produced local bulging, with no significant change in the spirally stiffened ribs (Figure 6d).

Compared with specimen Z1, the local buckling of the square steel tube was significantly weakened under the effect of the spiral rib restraint.

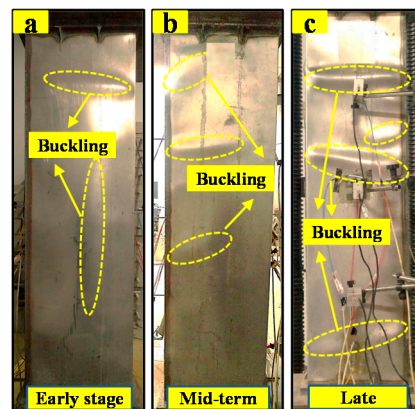


Figure 5. Z1 destruction phenomenon. (a) Early stage (b) medium stage (c) Late stage.

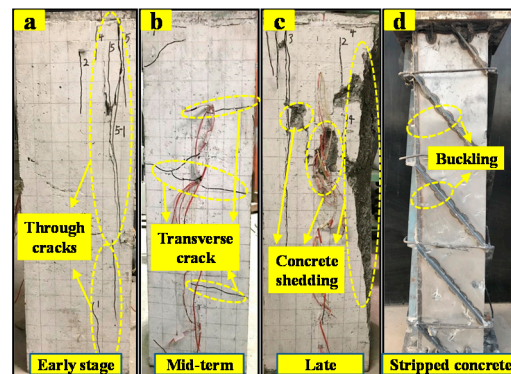


Figure 6. Z2 destruction phenomenon. (a) Early stage (b) medium stage (c) Late stage (d) Stripped concrete.

Specimen Z3 is a spiral rib-reinforced thin-walled concrete-filled steel tubular laminated column. The test procedure was as follows: When loaded to 970 kN, vertical cracks of approximately 30 mm in length appeared on the compressed side. At the same time, vertical cracks of approximately 15 mm in length were produced on the compressed side of faces B and D (Figure 7a). When the load was increased to 1420 kN, a vertical crack of about 30 mm was produced on the lower part of the compressed side (side B). When the ultimate load was approached, a transverse crack appeared on the tensile side at about 220 mm from the top of the column, and the concrete wrapped around the compressed area began to spall (Figure 7b). When the load reached the ultimate bearing capacity, the crack on the upper part of the tensile side extended from both sides to sides B and D, and a new transverse crack was produced in the middle of the specimen (Figure 7c). At the end of the test, after stripping the external concrete, it was found that the steel tube on the compressive surface had undergone a slight buckling, the spiral rib had undergone no obvious deformation, and the reinforcement was bent and deformed (Figure 7d). Compared to the Z2 specimen, the external concrete cracking was better controlled with the external reinforcement set in conjunction with the spiral ribs.

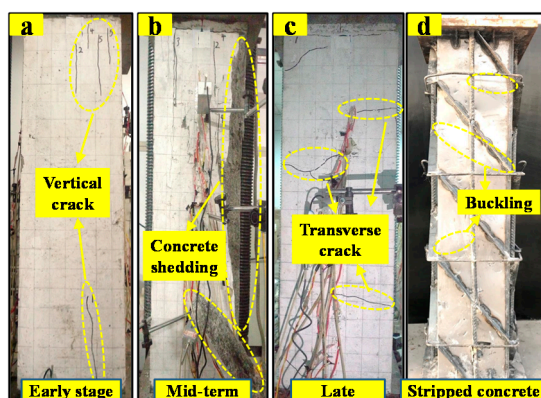


Figure 7. Z3 destruction phenomenon. (a) Early stage (b) medium stage (c) Late stage (d) Stripped concrete.

Specimen Z4 was a spiral rib-vertical plate thin-walled concrete-filled steel tubular laminated column. The test process is as follows: When loaded to 800 kN, cracks appeared at the top and bottom of the loaded surface of the laminated column (Figure 8a). As the load increased, the cracks gradually increased in length, and when the ultimate load was reached, the concrete in the stressed area formed through cracks, accompanied by the phenomenon of shedding (Figure 8b). When the load was further increased, transverse cracks appeared at 150 mm from the top of the column in the concrete on the tension surface (Figure 8c). At the end of the test, after stripping the concrete, it was found that the middle of the steel tube on the compression side of the specimen showed local bulging, and the vertical plate in the compression area also showed significant deformation (Figure 8d). Compared with specimen Z3, the steel pipe buckled in a similar form, with slight local deformation, and the external concrete produced mainly vertical cracks in the compression zone and transverse cracks in the tension zone.

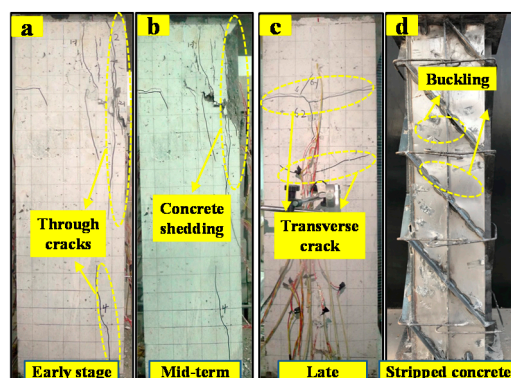


Figure 8. Z4 destruction phenomenon. (a) Early stage (b) medium stage (c) Late stage (d) Stripped concrete.

In summary, through the eccentric pressure tests, ordinary thin-walled steel pipe concrete pressure zone significantly bulged, spiral rib-reinforced thin-walled concrete-filled steel tubular laminated component failure modes for the external concrete pressure zone were crushed, tension zones showed transverse cracking, the buckling of thin-walled steel tube with spiral ribs was relatively slight, and the local stability of steel tube was enhanced.

3.2. Analysis of Test Results

3.2.1. Load–Displacement Curves

The load–displacement curves for each specimen are shown in Figure 9, and the characteristic values of load and displacement are listed in Table 4. The peak loads of columns Z2 and Z1 are similar, but the stiffness decayed faster in the later stages. Specimen Z3 had a vertical reinforcement set in the external concrete, the yield load and peak load

were both increased by about 18%, and the overall ductility was better. Z4 had a vertical slab set in the external concrete, the ultimate load capacity increased by about 11%, but a reduction in deformation capacity occurred in the later stages. Among them, the yield load in Figure 9 is taken as 75% of the peak load [39], which means that the steel tube yields when it enters the elastic–plastic stage. Overall, specimen Z3 has the best performance in terms of load capacity margin, deformation capacity, and safety reserve.

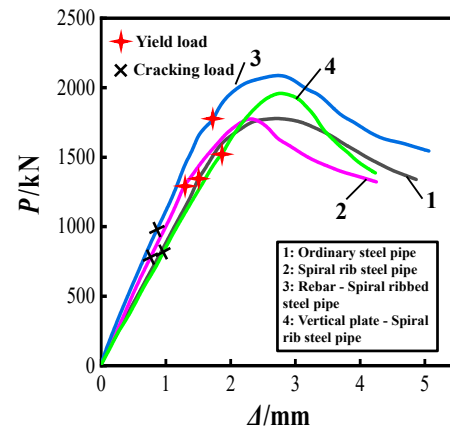


Figure 9. Comparison of load–displacement curves.

Table 4. Load and displacement eigenvalues.

| Test Piece | P_{cr}/kN | P_{cr}/P_u | P_y/kN | Δ_y/mm | P_{max}/kN | Δ_{max}/mm | P_u/kN | Δ_u/mm | Δ_u/Δ_y | Δ_u/Δ_{max} |
|------------|-------------|--------------|----------|---------------|--------------|-------------------|----------|---------------|---------------------|-------------------------|
| Z1 | - | - | 1344.9 | 2.04 | 1775.1 | 2.56 | 1508.8 | 4.16 | 2.04 | 1.625 |
| Z2 | 780 | 0.52 | 1303.6 | 1.83 | 1763.4 | 2.29 | 1498.9 | 3.35 | 1.83 | 1.463 |
| Z3 | 970 | 0.55 | 1765.7 | 1.98 | 2093.3 | 2.62 | 1779.3 | 3.97 | 2.01 | 1.515 |
| Z4 | 800 | 0.48 | 1526.4 | 2.23 | 1964.6 | 2.78 | 1669.9 | 3.71 | 1.66 | 1.335 |

Z2 is a single spiral rib constraint member, and the overall mechanical performance is poor because the development of external concrete cracks is rapid under the combined influence of vertical load and transverse deformation of steel tubes. Due to the external concrete accounting for about 40% of the whole cross-sectional area, the crack development is too rapid, resulting in a significant loss of overall stiffness of the component, resulting in the rapid reduction of bearing capacity. The spatial stability of the spiral rib was improved after the external reinforcement was added to the steel tube of specimen Z3. Meanwhile, spiral ribs and reinforced concrete are effectively segmented to form a spatial constraint system, which significantly reduces the rate of concrete crack penetration, improves the integrity of components, and gives full play to the mechanical properties. The Z4 specimen has a vertical plate on the outside of the steel tube, and the restraint system formed by the spiral ribs reduces the ability to control the cracking of the external concrete, leading to a rapid degradation of the stiffness and a reduction in the overall force performance at a later stage. It was found that for the concrete-filled steel tubular members, the ability of the external concrete to work with the core member has a greater effect on the overall strength of the member, and once cracking occurs early, it causes a rapid deterioration of the overall strength.

Overall, the spiral rib as a spatial restraint stiffening rib system can better restrain the buckling of such thin-walled steel pipes, significantly reduce the degree of buckling, and reduce the transverse deformation of the steel pipe. For thin-walled concrete-filled steel tubular members, force performance control should focus on the need to reduce the effects of local buckling and prevent the local instability of the steel pipe, leading to serious degradation of the bearing performance. On the other hand, there is a need to

ensure that the external concrete and the core members work together; once the two fail to work together, a rapid degradation of the stiffness and load capacity of the member occurs. The joint action of steel bars and spiral ribs can have a good segmentation effect on external concrete, and the crack development is significantly delayed, which improves the cooperative workability of external concrete and core components.

3.2.2. Load–Strain Curves

Before starting the test, grind and paste the strain gauge on the steel and the concrete surface. The size of the steel strain gauge is calculated as follows: base length multiplied by the base width is 6.9×3.6 mm; the size of the concrete strain gauge is the base length multiplied by the base width and is 92×5 mm. The strain of each part is analyzed as follows.

(a) Steel tube strain

The longitudinal strains in the steel tubes of each specimen were analyzed (Figure 10). The Z1 specimen of plain steel tube concrete showed the greatest strain rate in the compressive and tensile zones, indicating that it was subjected to higher loads, while the steel tubes of the laminated elements were subjected to relatively small forces. Among them, specimens Z2 and Z4 had similar strain patterns, and the strain rate in specimen Z3 is higher, indicating that the steel tube bearing contribution is improved under the spiral rib–steel restraint. According to the material test results, the material yield strain is about $1350 \mu\epsilon$, the peak strain of ordinary steel pipe in the compression zone is about $800 \mu\epsilon$, and in spiral rib members the strain exceeded $1100 \mu\epsilon$. The tensile zones formed a similar pattern, the peak strain in the ordinary steel pipe is about $1400 \mu\epsilon$ (reaching the yield strain); with a spiral rib added, the strain in the steel pipe exceeded $3000 \mu\epsilon$, leading to the strengthening phase, the material performance can be more fully mobilized.

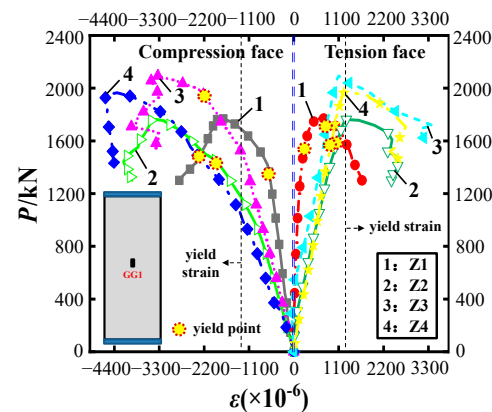


Figure 10. Steel tube load–longitudinal strain curve.

(b) Spiral rib strain

The helical rib load–strain curve is shown in Figure 11. Under eccentric compression, the strain in the spiral rib and its distribution in the compression zone and the tension zone is similar. Before reaching the yield load, the strain in the helical rib is small (about $200 \mu\epsilon$), and both are under compression. When the member yields, it rapidly transforms into a tensile state, and the strain increases rapidly, reaching about $1000 \mu\epsilon$, leaving the whole system in an elastic state. This arose because, before yielding, the lateral deformation of the steel pipe is small, and the spiral rib makes little contribution to the vertical load, so the strain therein is small. When the specimen enters the elastic–plastic stage, the core concrete is damaged, the lateral deformation of the steel pipe increases, and the spiral rib laterally constrains the steel pipe and is then under tension. Through the above analysis, it was deduced that: Spirally stiffened ribs act as a space spring-type structure. Their stiffness is

small, they do not bear the vertical load, and their role is mainly to enter the elastic–plastic stage of the later transverse deformation of the steel tube and restrain local buckling.

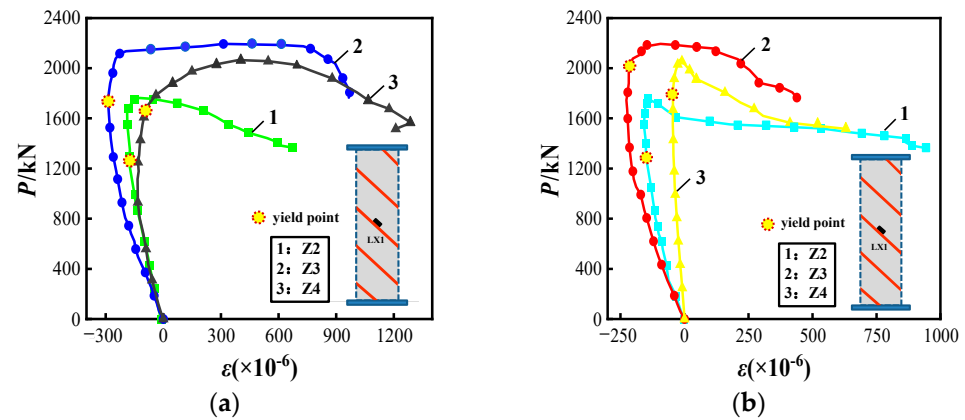


Figure 11. Load–strain relationship in the spiral rib: (a) Strain in the compression zone; (b) Strain in the tensile zone.

(c) Strain in the steel bar and vertical plate

Reinforcing bars and vertical plates are used as external concrete restraining members, and the load–strain curve is shown in Figure 12. Before the specimen reaches the ultimate load, the changes in strain are similar. When the peak load is exceeded, the steel bars can continue to bear load, but the vertical plate loses its effectiveness due to its high stiffness.

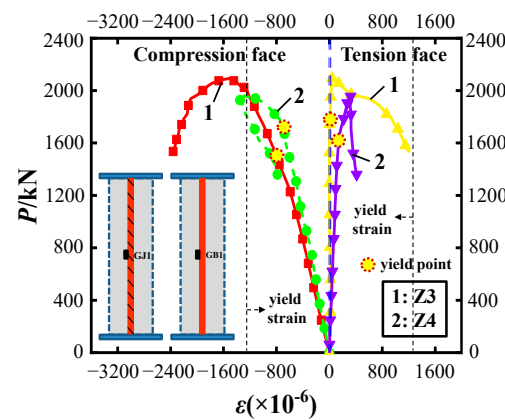


Figure 12. Comparison of load–strain curves of reinforcement and vertical plate.

(d) External concrete strain

The external concrete strains in the middle of the specimen are shown in Figure 13. After the concrete strain in the compressed zone reached $400 \mu\epsilon$, it entered the elastic–plastic stage when micro-cracks appeared in the concrete; that is, plastic deformation occurs. As the loading continues, the concrete gradually cracks until it falls off; the concrete in the tension zone cracked but did not spall, the vertical load was mainly borne by the internal steel part, and the strain could still increase.

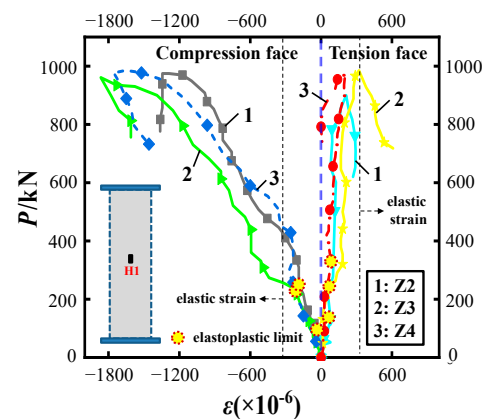


Figure 13. Load–strain curve of concrete.

3.3. Failure Mechanism

3.3.1. Failure Sequence

The sequence of failure was studied by comparing the strain relationships between the different parts of the specimens (Figure 14). For specimen Z2: In the elastic phase, the external concrete and steel tube were jointly stressed, the spiral rib essentially did not participate in this process; subsequently, the concrete broke down and played no further role, and the core steel tube concrete bore the load. After the peak load was reached, the strain in the spiral rib started to increase, but soon after, it played no further role. This is in general agreement with the overall force performance of specimen Z2.

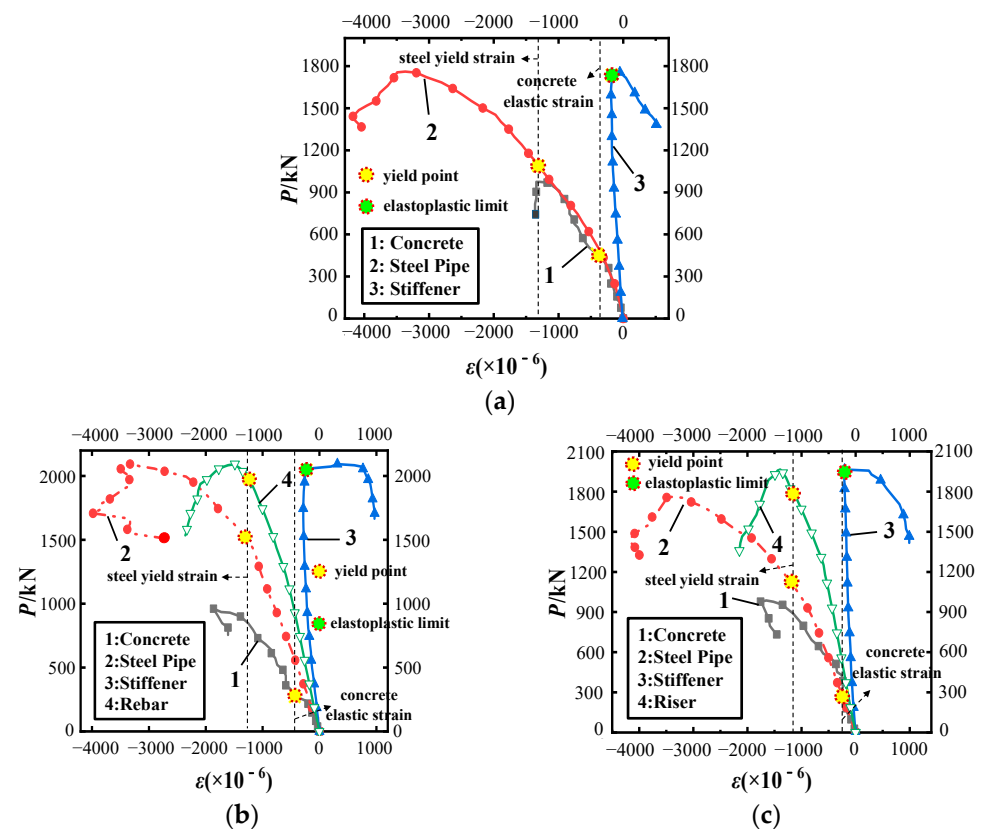


Figure 14. Load–strain relationship curves. (a) Specimen Z2; (b) Specimen Z3; (c) Specimen Z4.

For specimen Z3: In the elastic stage, the reinforcement, concrete, and steel pipe were jointly stressed; the strain in the spiral rib was small and plays a minor load-bearing role.

Consequently, the external concrete damage developed, and the steel parts and steel pipe continued to carry out work. After reaching the ultimate bearing capacity, spiral rib tension began to play a role, and the three worked together at this stage. As the load increased, the steel pipe flexed, the reinforcement was destroyed, the specimen failed as a whole, and the spiral rib remained in an elastic state throughout the test. For specimens Z3 and Z4, the failure processes were similar; the difference is that the steel plate strain increased more. From the above analysis, the failure sequence of this new laminated element is presented as follows: firstly, the external concrete fails; secondly, the steel tube and reinforcement (vertical plate) are damaged; and finally, the spiral rib plays no further role.

3.3.2. Stress Model

The mechanical behavior of the spiral rib-reinforced concrete-filled thin-walled steel tubular composite column was evaluated. The test eccentricity was 0.4, and the failure mode was still dominated by compressive failure. The external concrete was divided by spiral ribs, forming an oblique strip distribution area. The stirrups and steel bars across a grid limited their cracking and shedding. Finally, under the vertical load, the compression shear failure along the direction of the spiral rib occurred, and the main crack is similar to the angle of the spiral rib. The steel tube was also divided into inclined plate areas by spiral ribs, and the vertical load was decomposed into a pressure perpendicular to the long edge of the thin plate and a shear force parallel to the spiral ribs. The transverse tensile force was decomposed into the pressure perpendicular to the short edge of the thin plate and the parallel shear force. The stress mode is illustrated in Figure 15. Through the analysis, it was found that the thin-walled steel tube is divided into several oblique compression shear zones under the constraint of spiral ribs. Due to the large angle stiffness, the thin-walled steel tube was regularized and simplified as a rectangular thin plate. The boundary conditions were considered simply by being supported on four sides. The force was mainly vertical pressure, and the central part of the thin plate was bulging under compression shear. The stress model lays the foundation for further calculations of the buckling bearing capacity of the thin plate under spiral rib constraint.

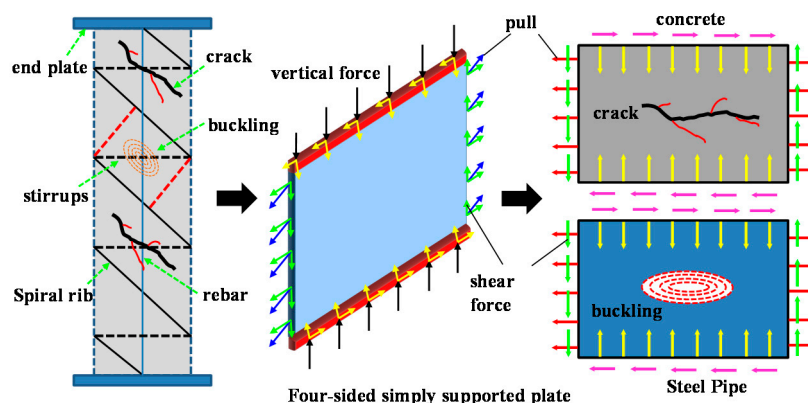


Figure 15. Stress model of specimen Z3.

3.4. Finite Element Analysis

3.4.1. Finite Element Module Method

(1) Material properties

According to the literature [40,41], the finite element analysis is carried out using Abaqus software [42]. The isotropic elastic–plastic model satisfying the Von Mises yield criterion was used for the steel principal structure relationship, and the four-stage secondary plastic flow model was used for the stress–strain relationship; the modulus of elasticity and Poisson’s ratio are taken as 2.06×10^5 MPa and 0.3, respectively. According to the results of the steel material testing, the double restraint effect of the spiral rib and core concrete was considered; the local stability enhancement factor α_1 was introduced into the yield

strength and ultimate strength of the steel tube, with a value of 1.15. The adjusted model is described as follows:

$$\sigma = \begin{cases} E_s \varepsilon_a & 0 \leq \varepsilon_a < \varepsilon_1 \\ \alpha_1 f_y & \varepsilon_1 \leq \varepsilon_a < \varepsilon_2 \\ f_y + \frac{\varepsilon_a - \varepsilon_2}{\varepsilon_3 - \varepsilon_2} (f_u - f_y) & \varepsilon_2 \leq \varepsilon_a < \varepsilon_3 \\ \alpha_1 f_u & \varepsilon_a \geq \varepsilon_3 \end{cases} \quad (1)$$

The plastic damage model is adopted for the external concrete; the strength is reduced due to the influences of the internal spiral rib extrusion and the lateral deformation of the steel pipe. The influence coefficient α_2 of concrete local extrusion is introduced (with a value of 0.75), and the modified model constitutive is as follows:

$$\sigma_c = \begin{cases} f_c \left[1 - \left(1 - \frac{\varepsilon_c}{\varepsilon_0} \right)^n \right] & \varepsilon_c \leq \varepsilon_0 \\ \alpha_2 f_c & \varepsilon_0 \leq \varepsilon_c \leq \varepsilon_{cu} \end{cases} \quad (2)$$

The core concrete was modeled using an enhanced uniaxial compressive stress–strain relationship; the restraint on the concrete within it can be increased as the steel pipe is limited by the lateral deformation of the spiral ribs. Corrections were made to the strain ε_0 corresponding to the peak concrete stress and the parameter β_0 for the descending section of the curve. The modulus of elasticity is calculated using the equation $E = 4730\sqrt{f_c}$. The Poisson's ratio is taken as 0.2:

$$y = \begin{cases} 2x - x^2 & (x \leq 1) \\ \frac{x}{\beta_0(x-1)^\eta + x} & (x > 1) \end{cases} \quad (3)$$

where:

$$\varepsilon_0 = \varepsilon_c + 800\zeta_1^{0.2}(1 + 24\zeta) \times 10^{-6} \quad (4)$$

$$\beta_0 = \frac{f_c^{0.1}}{1.2\sqrt{1 + \zeta_1}\sqrt{1 + \zeta}} \quad (5)$$

with, $x = \frac{\varepsilon_c}{\varepsilon_0}$, $y = \frac{\sigma_c}{\sigma_0}$, $\sigma_0 = f_c$, $\eta = 1.6 + \frac{1.5}{x}$, $\varepsilon_c = (1300 + 12f_c) \times 10^{-6}$, $\zeta_1 = \frac{A_s f_y}{A_c f_{ck}}$, and $\zeta = \frac{A_s f_y}{\alpha_s b_s f_{ck}}$.

(2) Modeling

The square steel tube and the spiral rib use a four-node reduced-integration shell element (S4R). This element can automatically select the thin or thick shell theory with the change of shell thickness during the solution. In addition, the Simpson integral of nine critical points is selected on the thickness to ensure the accuracy requirements. The solid element is suitable for an extensive deformation analysis, and the calculation accuracy is high. When the bending deformation of the grid occurs, the analysis accuracy is not significantly affected. Therefore, the loading end plate and concrete are selected to use the three-dimensional solid element (C3D8R) with an eight-node reduction integral scheme. The slenderness of the steel bar is relatively large; its bending, shearing and torsion effects are ignored, and only the tensile force is considered, so the truss element (T3D2) is used.

When the model is established, each material is non-linear and independent of each other; the steel tube and concrete are surface–surface contacts, and the friction coefficient in the tangential direction is 0.3; normal behavior adopts a hard contact without considering bond–slip between the concrete and the steel tube. The contact relationship between other parts is such that binding constraints are adopted between the steel pipe, the helical rib, and the vertical steel bar. The loads, displacements, and boundary conditions of the finite element model were all consistent with those pertaining to the test specimen (Figure 16).

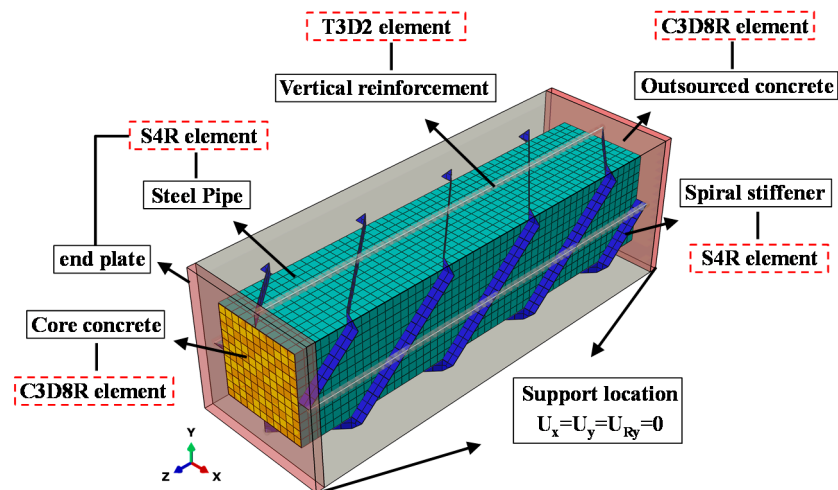


Figure 16. The finite element model of specimen Z3.

3.4.2. Validation Model

The damage pattern of specimen Z3 was obtained by finite element analysis (Figure 17). The central steel tube experienced significant flexural deformation, which is in general agreement with the test performance. The external reinforcement of the model is damaged, and the extent and amount of bending is slightly greater than that in the test. The external concrete of the model forms an oblique 45° failure area in the middle of the component, which is similar to the failure of the external concrete in the test. The load–displacement curves are compared (Figure 18). The peak load error is about 4%; the trends in the load–displacement curves of the two are similar. In summary, the model can better reflect the damage mode and force performance of a reinforced spirally ribbed concrete-filled steel pipe under eccentric compression.

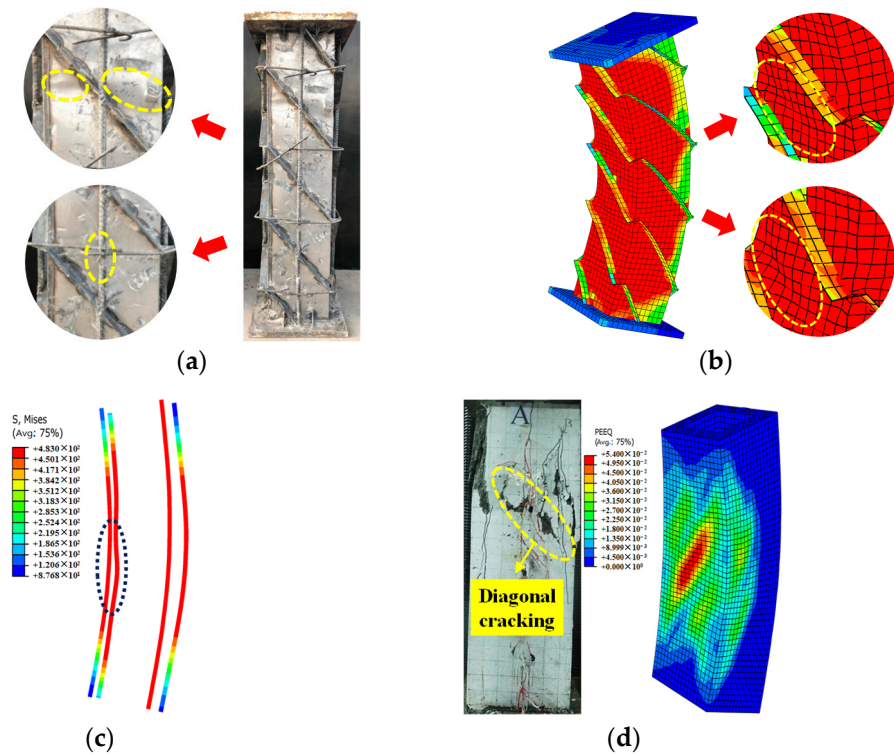


Figure 17. Finite element model loading and test comparison of specimen Z3. (a) Steel pipe and steel bar test phenomenon; (b) Buckling simulation of a spirally ribbed steel pipe; (c) Buckling simulation of steel bar; (d) Concrete failure simulation.

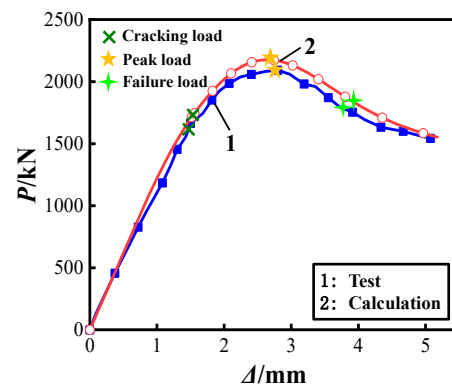


Figure 18. Comparison of load–displacement curves of specimen Z3.

3.5. Parametric Analysis

Based on the experimental verification model, a parametric analysis of each full-scale component was conducted. The influences of the width to thickness ratio of the spiral rib, width to thickness ratio of steel pipe, pitch, diameter of vertical reinforcement, and eccentricity were considered. The specific parameters are listed in Table 5.

Table 5. Model parameters.

| Specimen Number | b_s/mm | t_s/mm | b_s/t_s | d_0/mm | t_0/mm | d_0/t_0 | p/mm | d_1/mm | e_0/r_c |
|-----------------|----------|----------|-----------|----------|----------|-----------|--------|----------|-----------|
| LX1 | 90 | 6 | 15.0 | 660 | 3 | 220 | 3000 | 14 | 0.4 |
| LX2 | 90 | 8 | 11.25 | 660 | 3 | 220 | 3000 | 14 | 0.4 |
| LX3 | 90 | 10 | 9 | 660 | 3 | 220 | 3000 | 14 | 0.4 |
| LX4 | 90 | 14 | 6.4 | 660 | 3 | 220 | 3000 | 14 | 0.4 |
| LX5 | 60 | 8 | 7.5 | 660 | 3 | 220 | 3000 | 14 | 0.4 |
| LX6 | 110 | 8 | 13.75 | 660 | 3 | 220 | 3000 | 14 | 0.4 |
| GH1 | 90 | 8 | 11.25 | 660 | 1.5 | 440 | 3000 | 14 | 0.4 |
| GH2 | 90 | 8 | 11.25 | 660 | 2 | 330 | 3000 | 14 | 0.4 |
| GH3 | 90 | 8 | 11.25 | 660 | 3 | 220 | 3000 | 14 | 0.4 |
| GH4 | 90 | 8 | 11.25 | 660 | 4 | 165 | 3000 | 14 | 0.4 |
| GH5 | 90 | 8 | 11.25 | 660 | 5 | 132 | 3000 | 14 | 0.4 |
| LJ1 | 90 | 8 | 11.25 | 660 | 4 | 165 | 2400 | 14 | 0.4 |
| LJ2 | 90 | 8 | 11.25 | 660 | 4 | 165 | 3000 | 14 | 0.4 |
| LJ3 | 90 | 8 | 11.25 | 660 | 4 | 165 | 3600 | 14 | 0.4 |
| LJ4 | 90 | 8 | 11.25 | 660 | 4 | 165 | 4500 | 14 | 0.4 |
| SG1 | 90 | 8 | 11.25 | 660 | 4 | 165 | 4500 | 10 | 0.4 |
| SG2 | 90 | 8 | 11.25 | 660 | 4 | 165 | 4500 | 14 | 0.4 |
| SG3 | 90 | 8 | 11.25 | 660 | 4 | 165 | 4500 | 18 | 0.4 |
| SG4 | 90 | 8 | 11.25 | 660 | 4 | 165 | 4500 | 22 | 0.4 |
| SG5 | 90 | 8 | 11.25 | 660 | 4 | 165 | 4500 | 25 | 0.4 |
| SG6 | 90 | 8 | 11.25 | 660 | 4 | 165 | 4500 | 28 | 0.4 |
| PX1 | 90 | 8 | 11.25 | 660 | 4 | 165 | 4500 | 22 | 0.3 |
| PX2 | 90 | 8 | 11.25 | 660 | 4 | 165 | 4500 | 22 | 0.4 |
| PX3 | 90 | 8 | 11.25 | 660 | 4 | 165 | 4500 | 22 | 0.5 |
| PX4 | 90 | 8 | 11.25 | 660 | 4 | 165 | 4500 | 22 | 0.6 |
| PX5 | 90 | 8 | 11.25 | 660 | 4 | 165 | 4500 | 22 | 0.8 |
| PX6 | 90 | 8 | 11.25 | 660 | 4 | 165 | 4500 | 22 | 0.9 |
| PX7 | 90 | 8 | 11.25 | 660 | 4 | 165 | 4500 | 22 | 1.0 |
| PX8 | 90 | 8 | 11.25 | 660 | 4 | 165 | 4500 | 22 | 1.2 |
| PX9 | 90 | 8 | 11.25 | 660 | 4 | 165 | 4500 | 22 | 1.4 |

3.5.1. Width to Thickness Ratio of the Spiral Rib

Through a parametric analysis, it was found that the overall bearing capacity and deformation capacity of each model are not significantly different (Figure 19). When the width of the spiral rib was constant, the bearing capacity and ductility decreased by about 5%, with an increase in thickness. Under the condition of constant spiral rib thickness, with the increase in width, the mechanical performance of the component first slightly increases and then remains unchanged; however, when the width to thickness ratio is too small, this leads to spiral rib stress that is too large and not conducive to achieving the desired constraint. In summary, the spiral rib has little effect on the stiffness of the component, and its effect is mainly to limit lateral deformation. However, the increase in the thickness of the spiral rib (reduced width to thickness ratio) impedes the eccentric compression performance. Through an analysis, the recommended range of values for the width to thickness ratio of spiral ribs is 11 to 15.

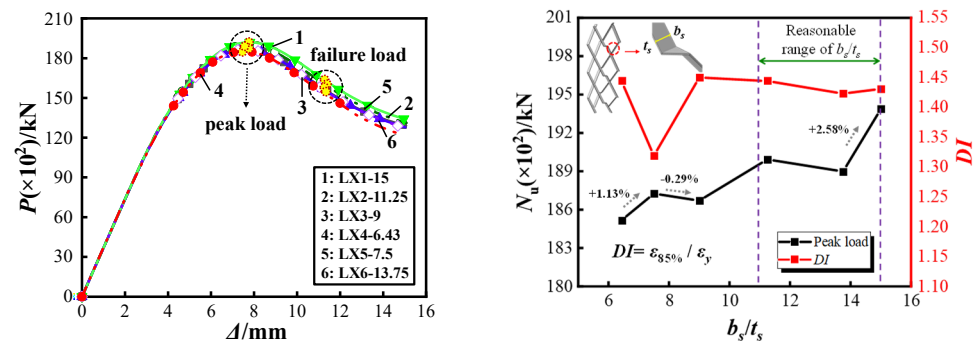


Figure 19. Load–displacement curves for different width to thickness ratios of spiral ribs.

3.5.2. Width to Thickness Ratio of the Steel Tube

A parametric analysis of the steel tube width to thickness ratio was conducted to observe the effect on the force performance of the models. The load–displacement curve is shown in Figure 20, and the parametric analysis indicated that the overall load-carrying capacity and deformation capacity of the models vary considerably. Under the condition that the width of the steel pipe remains unchanged, the load-carrying capacity and ductility of the model increase by about 15% and 9%, respectively, as the thickness increases; the greater the thickness of the steel pipe, the greater the increase in load-carrying capacity and ductility. In summary, the width to thickness ratio of steel pipes has a greater effect on the bearing capacity of the member, mainly limiting the core concrete deformation and improving the bearing capacity of the member. However, when the width to thickness ratio of steel tubes is too small, this affects the cost of the process. Because the stiffening ribs lose their effectiveness, in a thin-walled concrete-filled steel tubular laminated members, the width to thickness ratio of the steel tube is recommended to be between 165 and 220.

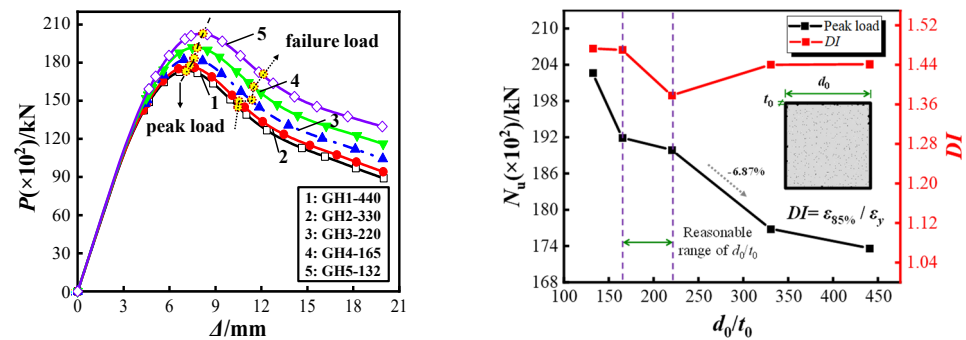


Figure 20. Load–displacement curves for different tube width to thickness ratios.

3.5.3. Pitch

A parametric analysis of the pitch was conducted (Figure 21). The results show that: the angle at which the spiral rib is set determines its density, and the smaller the pitch, the lower the stress to which it is subjected. When the spiral rib is close to the horizontal state, the transverse restraint is stronger, the ring hoop effect is significant, and the ductility is about 38% higher than in other models; however, the ultimate bearing capacity is not greatly improved. The larger the pitch, the greater the axial action, and the closer the stresses are to those on traditional vertical plate stiffening ribs. In summary, considering that the spiral rib mainly acts as a circular constraint, the pitch is recommended to be between H and 1.2H.

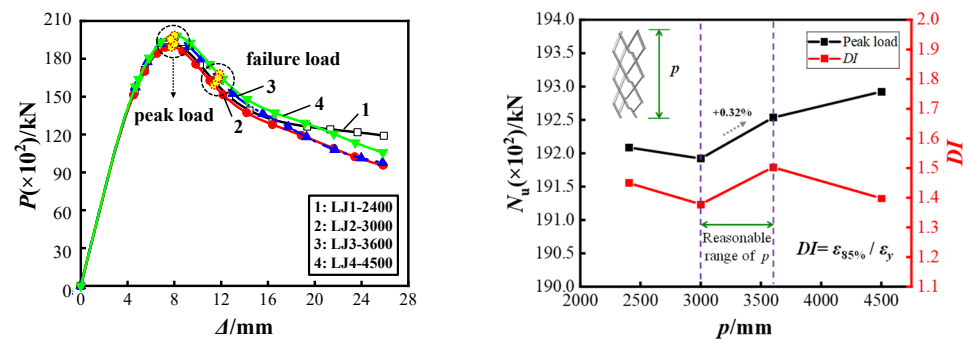


Figure 21. Load–displacement curves with different pitches.

3.5.4. Vertical Steel Bar Diameter

A parametric analysis of the vertical reinforcement diameters was conducted (Figure 22), showing that the diameter of the reinforcement has no significant effect on the overall load-bearing capacity and ductility. However, too large or too small a diameter of reinforcement will affect the cracking of the external concrete, thus affecting the overall load-bearing performance. Reinforcing bars are used as external concrete construction measures. Overall, it is recommended that the spacing should not be greater than 250 mm, and the diameter of the reinforcing bars should be 7/100 to 11/100 of the spacing.

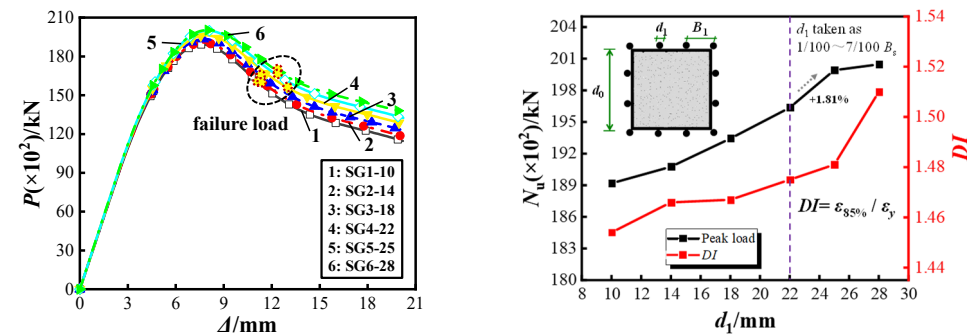


Figure 22. Load–displacement curves for different reinforcement diameters.

3.5.5. Eccentricity

A parametric analysis of the effect of eccentricity was conducted, and the load–displacement curve is shown in Figure 23. The parametric analysis revealed that the overall load-carrying capacity and deformation capacity of the models with different eccentricities differed significantly. The analysis found that: as the eccentricity increases, the ductility increases by about 50%, but the bearing capacity decreases by 35%. The greater the eccentricity, the more the member is affected by the bending moment, the lower the axial stiffness and ultimate bearing capacity, the better the later ductility. The smaller the eccentricity, the closer to the axial bearing state, the higher the ultimate bearing capacity, but the poorer the deformation capacity. In summary, the eccentricity should not be greater than 0.5 for this new combined type of member.

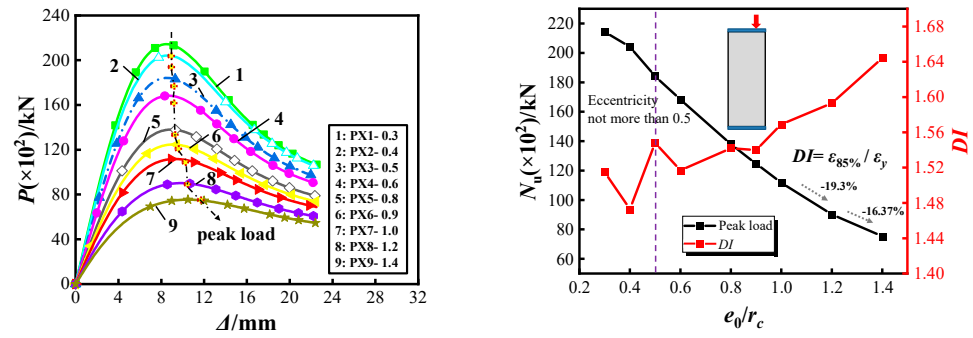


Figure 23. Load–displacement curves with different eccentricities.

The N–M relationship curve for the model column was obtained from the calculation results (Figure 24). As the eccentricity increases to around 0.9, the curve turns, signifying a shift from small eccentric compressive damage to large eccentric damage. When analyzing the N–M relationship curves for different pitches (Figure 25), increasing both the spiral rib density and the spiral rib angle is found to enhance the bias resistance of the laminated member to a small extent.

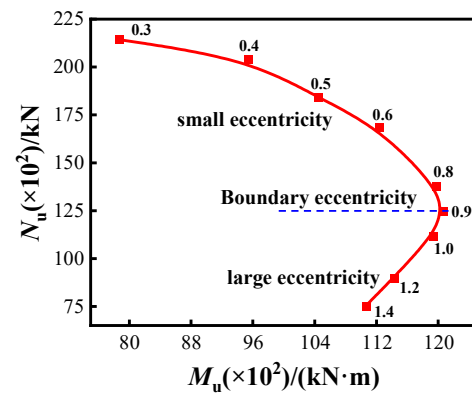


Figure 24. N–M curves of different eccentricities.

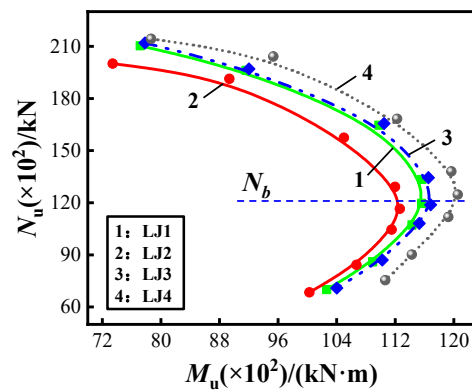


Figure 25. N–M curves for different pitches.

3.6. Bearing Capacity Calculation

The bearing capacity of thin-walled square concrete-filled steel tubular composite columns with spiral ribs and steel bars is calculated and evaluated. According to the theory of superposition, the bearing capacity of the superimposed column is mainly composed of four parts: vertical reinforcement N_1 , external concrete N_2 , spirally ribbed steel pipe N_3 , and core concrete N_4 .

The bearing capacity of reinforcement is determined by its strength and cross-sectional area and is calculated as follows:

$$N_1 = A_{s1} \times f_{y1} \quad (6)$$

The external concrete is mainly determined by its compressive strength and cross-sectional area, which is reduced due to the loading process by the extrusion of the spiral ribs and the lateral deformation of the steel pipe. The concrete strength reduction factor α_2 is introduced and, according to the test, the value of 0.75 is taken to obtain:

$$N_2 = \alpha_2 \times A_{c1} \times f_{ck} \quad (7)$$

For the spirally ribbed steel pipe bearing capacity N_3 , the effect of thin-walled steel pipe stability under spiral rib constraints is considered via the introduction of a spirally ribbed steel pipe bearing capacity impact coefficient β . Among these, β is affected by the helical rib width to thickness ratio b_s/t_s , the pitch p , and the width to thickness ratio d_0/t_0 of the steel pipe according to the results of numerical analysis. Then the data are regressed to ascertain the trend therein (Figure 26). β is positively related to b_s/t_s and p and inversely related to d_0/t_0 . Taking its slope as the influence coefficient, β is given by:

$$\beta = 0.01b_s/t_s - 0.102d_0/t_0 + 0.046p \quad (8)$$

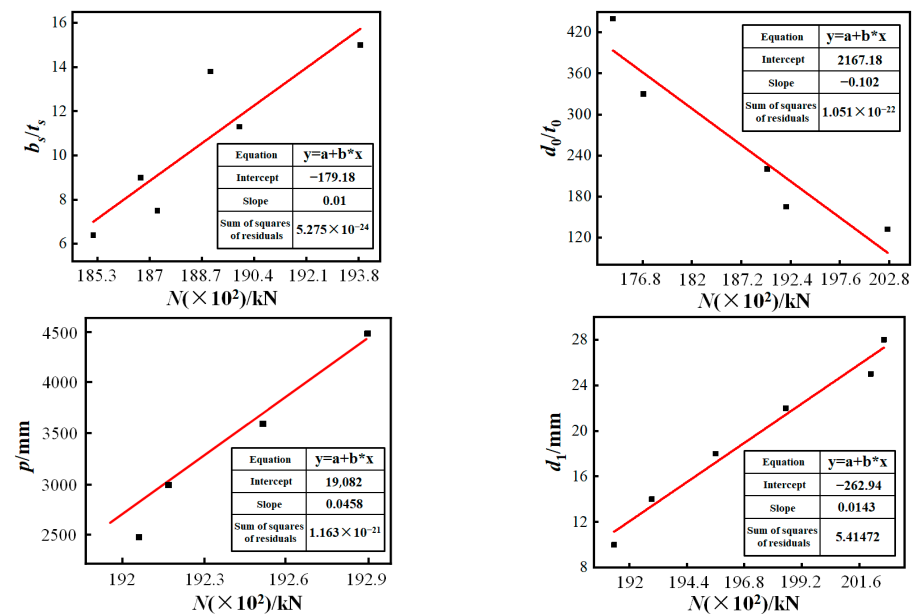


Figure 26. Regression analysis: key influencing factors.

The spirally ribbed steel pipe bearing capacity N_3 is given by:

$$N_3 = \beta \times A_{s2} \times f_y \quad (9)$$

The bearing capacity of core concrete N_4 is mainly obtained by its cross-sectional area and compressive strength. Considering the influence of the spiral ribbed steel pipe on the compressive strength of the core material, the core concrete intensification factor k under hoop restraint is introduced, and the value of k is mainly influenced by the spirally ribbed steel pipe sleeve factor ζ . Firstly, the comprehensive influence coefficient δ_1 of the strength of composite column thin-walled steel tube is calculated; δ_1 is mainly affected by the spiral rib width to thickness ratio b_s/t_s , pitch p , the width to thickness ratio d_0/t_0 of the steel pipe and reinforcement diameter d_1 . According to the regression formula (Figure 26), the slope

of the fitted straight line of each influencing parameter is used as the calculation coefficient to obtain an expression for δ_1 :

$$\delta_1 = 0.01b_s/t_s - 0.102d_0/t_0 + 0.046p + 0.014d_1 \quad (10)$$

On this basis, the constraint factor ζ for spirally ribbed steel pipes is given by:

$$\zeta = \frac{A_s2f_y(1 + \delta_1)}{A_c2f_{ck}} \quad (11)$$

The reinforcement coefficient k is mainly affected by the constraint coefficient ζ of the spirally ribbed steel pipe. According to the numerical calculation results, the data are fitted (Figure 27). The calculation formula is:

$$k = 1 + 0.839\zeta^{0.149} \quad (12)$$

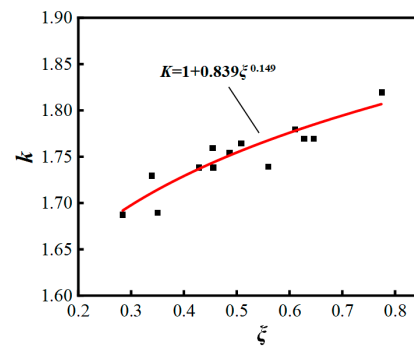


Figure 27. Fitting relationship between k and ζ .

The formula for the core concrete bearing capacity is as follows:

$$N_4 = k \times A_{c2} \times f_{ck} \quad (13)$$

Finally, the axial compressive bearing capacity formula of the superimposed column is obtained:

$$N_u = A_{s1}f_{y1} + \alpha_1A_{c1}f_{ck} + \beta A_{s2}f_y + kA_{c2}f_{ck} \quad (14)$$

Using the calculation formula proposed in [40] by way of modification, the eccentric compressive bearing capacity of the superimposed column is obtained:

$$N_e = \varphi_e N_u \quad (15)$$

$$\varphi_e = \frac{1}{1 + 1.85e_0/r_c} \quad (16)$$

Equation (16) is compared with the numerical calculation results (Table 6). The discrepancies are all within 10%, and the accuracy is high, so the formula can provide a basis for the calculation of the bearing capacity of the new composite member.

Table 6. Calculation results.

| Specimen Number | ζ | k | Analog Value/kN | Calculated/kN | Error % |
|-----------------|---------|-------|-----------------|---------------|---------|
| LX1 | 0.428 | 1.879 | 19,385.6 | 18,538.4 | 4.37 |
| LX2 | 0.486 | 1.803 | 18,992.9 | 18,691.3 | 1.58 |
| LX3 | 0.455 | 1.739 | 18,670.9 | 18,713.5 | 0.23 |
| LX4 | 0.559 | 1.690 | 18,517.0 | 18,988.2 | 2.54 |
| LX5 | 0.454 | 1.770 | 18,725.7 | 18,551.8 | 0.93 |
| LX6 | 0.508 | 1.780 | 18,898.3 | 18,784.8 | 0.60 |
| GH1 | 0.284 | 1.625 | 17,365.7 | 17,796.3 | 2.48 |
| GH2 | 0.350 | 1.649 | 17,687.8 | 18,101.8 | 2.34 |
| GH3 | 0.486 | 1.803 | 18,992.0 | 18,691.3 | 1.58 |
| GH4 | 0.627 | 1.770 | 19,192.1 | 19,269.3 | 0.40 |
| GH5 | 0.774 | 1.876 | 20,263.7 | 19,853.3 | 2.03 |
| LJ1 | 0.610 | 1.780 | 19,208.7 | 19,196.0 | 0.07 |
| LJ2 | 0.627 | 1.770 | 19,192.1 | 19,269.3 | 0.40 |
| LJ3 | 0.339 | 1.776 | 19,253.4 | 18,878.9 | 1.95 |
| LJ4 | 0.645 | 1.778 | 19,292.3 | 19,337.6 | 0.23 |

4. Conclusions

Through the study of eccentric loading tests, parametric analysis, and load-carrying capacity calculation of thin-walled square concrete-filled steel tubular laminated columns with different forms of restraint, the following conclusions were obtained:

- (1) Under the constraint of spiral rib, the buckling of the steel tube is limited to occurring between the stiffeners, oblique bulging occurs, and the extent of buckling is significantly decreased. Compared with an ordinary thin-walled steel pipe concrete column (Z1), the peak bearing capacity of the spiral rib–steel constraint composite member (Z3) increased by 17.9%, the problem of fire and corrosion resistance can be better solved, and the overall performance improved. For Z2 and Z4 specimens, the deformation capacity is reduced by 10.3% and 18.6%, respectively, compared to Z1, which shows that the comprehensive performance of the specimens with a single spiral rib and the vertical plate-spiral rib is not prominent, and the overall stiffness degradation of the component is accelerated. Therefore, the external spiral rib restraint form needs to be used in conjunction with vertical reinforcement.
- (2) A spiral rib can improve the local flexural stiffness and enhance the thin-walled steel tube flexural capacity. As a new type of spatial restraint system, its vertical stiffness is negligible; when the member enters the elastic–plastic phase, the steel tube lateral deformation increases, before the role of the overall deformation restraint is mobilized, which is different from the role played by traditional vertical stiffening ribs.
- (3) Through a parameter analysis, the following design suggestions are obtained: the width to thickness ratio of spiral rib reinforcement should be between 11 and 15 and the spacing should be between H and $1.2H$; the width to thickness ratio of the thin-walled steel pipe for this laminated member is between 165 and 220; the spacing of reinforcement as a construction component is recommended to be no more than 250 mm and the diameter of reinforcement should be $7/100$ to $11/100$ of the spacing $B1$; the eccentricity should not be greater than 0.5; through the N – M relationship, the limit of damage in compression and tension under eccentric loading is obtained as an eccentricity of about 0.9.
- (4) The influences of parameters, such as the bearing capacity influence coefficient β of the spirally ribbed steel pipe, reinforcement factor for core concrete under hoop restraint k , and the hoop coefficient ζ of the spirally ribbed steel pipe were determined, and the method of calculating the eccentric compressive ultimate bearing capacity of this new composite member was proposed, which can provide a basis for its engineering design.

Author Contributions: Conceptualization, Z.W. and Y.S.; methodology, Z.W. and Y.S.; software, Z.W.; validation, Z.W. and Y.S.; investigation, Y.S. and J.W.; resources, Z.W.; data curation, J.W.; writing—original draft preparation, Z.W. and Y.S.; writing—review and editing, J.L. and X.L.; visualization, Z.W. and Y.S.; supervision, Y.S. and X.L.; project administration, Z.W.; funding acquisition, Z.W. All authors have read and agreed to the published version of the manuscript.

Funding: Supported by the National Natural Science Foundation of China (51978571).

Institutional Review Board Statement: Not applicable.

Informed Consent Statement: Not applicable.

Data Availability Statement: Data are contained within the article.

Acknowledgments: This study was supported by the National Natural Science Foundation of China.

Conflicts of Interest: The authors declare that they have no conflict of interest.

Abbreviations

| | |
|-------------------------|--|
| H | Component height |
| d_0/t_0 | Tube edge length and thickness |
| $b_s \times t_s$ | Spiral rib width and thickness |
| α_s | Horizontal spacing of spiral ribs |
| b_s | Longitudinal spacing of spiral ribs |
| $b_p \times t_p$ | Vertical plate width and thickness |
| d_1 | Diameter of vertical reinforcement |
| p | Pitch |
| δ | Elongation |
| e_0/r_c | Load eccentricity |
| f_y | Steel yield strength |
| f_{y1} | Reinforcement yield strength |
| f_u | Ultimate strength of steel |
| f_y/f_u | Yield–strength ratio |
| $f_{cu,k}$ | Standard value of compressive strength of concrete cube |
| f_{ck} | Standard value of axial compressive strength of concrete |
| f_c | Design value of axial compressive strength of concrete |
| E_s | Elastic modulus of steel |
| E_c | Elastic modulus of concrete |
| P_{cr} | Cracking load |
| P_y | Yield load |
| P_{max} | Peak load |
| P_u | Limit load |
| P_{cr}/P_u | Cracking load ratio |
| Δ_y | Yield displacement |
| Δ_{max} | Peak displacement |
| Δ_u | Limit displacement |
| Δ_u/Δ_y | Deformation capacity |
| Δ_u/Δ_{max} | Security reserve |
| σ_c | Concrete stress |
| σ_0 | Peak stress of concrete |
| ε_a | Steel tube strain |
| ε_c | Concrete strain |
| ε_0 | Peak strain of concrete |
| ε_{cu} | Ultimate compressive strain of normal section concrete |
| η | Strain calculation parameters |
| ε_1 | Steel yield strain |
| ε_2 | Plastic strain of steel |
| ε_3 | Flow plastic strain of steel |
| α_1 | Local stability enhancement coefficient of steel pipe |
| α_2 | Strength reduction coefficient of concrete |

| | |
|-------------|--|
| δ_1 | Comprehensive influence coefficient of strength of thin-wall composite column steel pipe |
| k | Reinforcement coefficient of core concrete under hoop confinement |
| φ_e | Eccentricity impact coefficient |
| β | Influence coefficient of bearing capacity of spiral rib steel tube |
| β_0 | Strain curve drop correction factor |
| ξ | Constraint coefficient of spiral rib steel pipe |
| ξ_1 | The hoop coefficient of ordinary steel pipe |
| ζ | Spiral rib restraint factor |
| A_a | Steel pipe cross-sectional area |
| A_c | Full concrete cross-sectional area |
| A_s | Cross-sectional area of single spiral rib |
| A_{s1} | Rebar cross-sectional area |
| A_{s2} | Cross-sectional area of spiral ribbed steel pipe |
| A_{c1} | External concrete cross-sectional area |
| A_{c2} | Core concrete cross-sectional area |
| N_1 | Vertical steel bearing capacity |
| N_2 | External concrete bearing capacity |
| N_3 | Spiral ribbed steel pipe bearing capacity |
| N_4 | Core concrete bearing capacity |
| N_u | Axial compression ultimate bearing capacity |
| N_e | Bias ultimate bearing capacity |

References

- Heman Aiswarya, M.; Roshni, K.G. Numerical Study on Concrete-Filled Steel Tubes with Diagonal Binding Ribs and Longitudinal Stiffeners. *Recent Adv. Comput. Exp. Mech.* **2022**, *11*, 1524. [[CrossRef](#)]
- O'Shea, M.D.; Bridge, R.Q. Local buckling of thin-walled circular steel sections with or without internal restraint. *J. Constr. Steel Res.* **1997**, *41*, 137–157. [[CrossRef](#)]
- Thomas, J.; Sandeep, T.N. Experimental study on circular CFST short columns with intermittently welded stiffeners. *Steel Compos. Struct.* **2018**, *29*, 659–667. [[CrossRef](#)]
- Ansa, K.P.; Keerthi, S. Analysis of the Concrete Filled Steel Tubes with Diagonal Ribs. In *Proceedings of SECON 2020 Structural Engineering and Construction Management*; Springer: Cham, Switzerland, 2020; pp. 719–734. [[CrossRef](#)]
- Zhou, Z.; Gan, D.; Zhou, X.H. Improved Composite Effect of Square Concrete-Filled Steel Tubes with Diagonal Binding Ribs. *J. Struct. Eng.* **2019**, *145*, 04019112. [[CrossRef](#)]
- Chybiński, M.; Garstecki, A. Diagonal Versus Orthogonal Ribs in Stability of Steel I Beams. *Procedia Eng.* **2017**, *172*, 172–177. [[CrossRef](#)]
- Huang, H.; Zhang, A.G.; Li, Y.; Chen, M.C. Experimental research and finite element analysis on mechanical performance of concrete-filled stiffened square steel tubular stub columns subjected to axial compression. *J. Build. Struct.* **2011**, *32*, 75–82. [[CrossRef](#)]
- Huang, B.T.; Dai, J.G.; Weng, K.F.; Zhu, J.X.; Shah, S.P. Flexural Performance of UHPC–Concrete–ECC Composite Member Reinforced with Perforated Steel Plates. *J. Struct. Eng.* **2021**, *147*, 04021065. [[CrossRef](#)]
- Maiorana, E.; Tetougueni, C.D.; Zampieri, P.; Pellegrino, C. Experimental and numerical investigations on slender panels with holes under symmetrical localised loads. *Eng. Struct.* **2021**, *228*, 111323. [[CrossRef](#)]
- Wei, Y.; Wang, Z.Y.; Chen, S.; Zhao, K.; Zheng, K. Structural behavior of prefabricated bamboo-lightweight concrete composite beams with perforated steel plate connectors. *Arch. Civ. Mech. Eng.* **2021**, *21*, 15. [[CrossRef](#)]
- Pellegrino, C.; Maiorana, E.; Modena, C. Linear and non-linear behaviour of steel plates with circular and rectangular holes under shear loading. *Thin-Walled Struct.* **2008**, *47*, 607–616. [[CrossRef](#)]
- Hamidian, M.R.; Jumaat, M.Z.; Alengaram, U.J.; Sulong, N.R.; Shafiq, P. Pitch spacing effect on the axial compressive behaviour of spirally reinforced concrete-filled steel tube (SRCFT). *Thin-Walled Struct.* **2016**, *100*, 213–223. [[CrossRef](#)]
- Ibrahim, A.; Askar, H.S.; El, Z.M.E. Torsional Behavior of Solid and Hollow Concrete Beams Reinforced with Inclined Spirals. *J. King Saud Univ. Eng. Sci.* **2020**, *34*, 309–321. [[CrossRef](#)]
- Katkhuda, H.N.; Shatarat, N.K.; Al-Rakhameen, A. Improving the Torsional Capacity of Reinforced Concrete Beams with Spiral Reinforcement. *Int. J. Civ. Struct. Eng.* **2019**, *8*, 113–118. [[CrossRef](#)]
- Gunawardena, Y.; Aslani, F. Behaviour and design of concrete-filled spiral-welded stainless-steel tube short columns under concentric and eccentric axial compression loading. *J. Constr. Steel Res.* **2019**, *158*, 522–546. [[CrossRef](#)]
- Wu, B.; Zhang, Q.; Chen, G.M. Compressive behavior of thin-walled circular steel tubular columns filled with steel stirrup-reinforced compound concrete. *Eng. Struct.* **2018**, *170*, 178–195. [[CrossRef](#)]
- Zhang, Y.F.; Wang, Q.; Cai, C.S.; Yan, C. Calculation on Ultimate Axial Bearing Capacity of Concrete-Filled Square Steel Tubular Column with Spiral Stirrups. *J. Comput. Theor. Nanosci.* **2016**, *13*, 1422–1425. [[CrossRef](#)]

18. Xue, J.Y.; Zhao, X.B.; Ke, X.J.; Zhang, X.; Zhang, F.; Zhang, P. Experimental and numerical investigation of high-strength concrete encased steel columns with rectangular-spiral stirrups. *J. Build. Eng.* **2020**, *32*, 101518. [[CrossRef](#)]
19. Chen, Z.P.; Ke, X.J.; Chen, Y.L. Experimental study on seismic behavior of steel reinforced high-strength concrete columns confined by square spiral stirrups. *J. Chin. Civ. Eng. J.* **2015**, *48*, 41–49, +59.
20. Inai, E.; Mukai, A.; Kai, M.; Tokinoya, H.; Fukumoto, T.; Mori, K. Behavior of Concrete-Filled Steel Tube Beam Columns. *J. Struct. Eng.* **2004**, *130*, 189–202. [[CrossRef](#)]
21. Wu, Z.M.; Yang, S.T.; Zheng, J.J.; Hu, X. Analytical solution for the pull-out response of FRP rods embedded in steel tubes filled with cement grout. *Mater. Struct.* **2010**, *43*, 597–609. [[CrossRef](#)]
22. Zhang, Y.C.; Chen, Y. Experimental study and finite element analysis of square stub columns with straight ribs of concrete-filled thin-walled steel tube. *J. Build. Struct.* **2006**, *27*, 23–29. [[CrossRef](#)]
23. Le, K.B.; Cao, V.V. Numerical Study of Circular Concrete Filled Steel Tubes Subjected to Pure Torsion. *Buildings* **2021**, *11*, 397. [[CrossRef](#)]
24. Islam, M.M.; Ali, R.B.; Begum, M.; Rahman, S. Experimental Study of Square Concrete-Filled Welded Cold-Formed Steel Columns Under Concentric Loading. *Arab. J. Sci. Eng.* **2020**, *46*, 4225–4237. [[CrossRef](#)]
25. Ananthi, G.; Roy, K.; Lim, J. Experimental and numerical investigations on axial strength of back-to-back built-up cold-formed steel angle columns. *Steel Compos. Struct.* **2019**, *31*, 601–615. [[CrossRef](#)]
26. Wei, J.G.; Luo, X.; Lai, Z.C.; Varma, A.H. Experimental Behavior and Design of High-Strength Circular Concrete-Filled Steel Tube Short Columns. *J. Struct. Eng.* **2020**, *146*, 04019184. [[CrossRef](#)]
27. Hernández-Figueirido, D.; Romero, M.L.; Bonet, J.L.; Montalvá, J.M. Influence of Slenderness on High-Strength Rectangular Concrete-Filled Tubular Columns with Axial Load and Nonconstant Bending Moment. *J. Struct. Eng.* **2012**, *138*, 1436–1445. [[CrossRef](#)]
28. Wang, J.; Sun, Q.; Li, J. Experimental study on seismic behavior of high-strength circular concrete-filled thin-walled steel tubular columns. *Eng. Struct.* **2019**, *182*, 403–415. [[CrossRef](#)]
29. Zhou, S.; Sun, Q.; Wu, X. Impact of D/t ratio on circular concrete-filled high-strength steel tubular stub columns under axial compression. *Thin-Walled Struct.* **2018**, *132*, 461–474. [[CrossRef](#)]
30. Child, J.A.; Bowry, M.W.; Knowles, J.P. Abnormality of red-cell diameter-thickness ratio: Findings in iron-deficiency anaemia. *Br. J. Haematol.* **1970**, *19*, 251–255. [[CrossRef](#)] [[PubMed](#)]
31. Ci, J.C.; Chen, S.C.; Jia, H.; Yan, W.; Song, T.; Kim, K.-S. Axial compression performance analysis and bearing capacity calculation on square concrete-filled double-tube short columns. *Mar. Struct.* **2020**, *72*, 102775. [[CrossRef](#)]
32. Zhou, C.Y.; Yang, J.R.; Jiang, W.W. Transverse Ribs Affect the Stability of Steel-Concrete Composite Box Beams. *Appl. Mech. Mater.* **2014**, *3308*, 1663–1667. [[CrossRef](#)]
33. Higaki, S.; Nishida, H.; Koike, Y.; Sasada, M.; Tanaka, T. Effect of transverse ribs on axial displacement of rebars in bending. *Procedia Manuf.* **2020**, *50*, 253–256. [[CrossRef](#)]
34. Hasan, H.G.; Ekmekyapar, T. Mechanical Performance of Stiffened Concrete Filled Double Skin Steel Tubular Stub Columns under Axial Compression. *KSCE J. Civ. Eng.* **2019**, *23*, 2281–2292. [[CrossRef](#)]
35. Raza, A.; Ali, B.; Nawaz, M.A.; Ahmed, I. Structural performance of FRP-RC compression members wrapped with FRP composites. *Structures* **2020**, *27*, 1693–1709. [[CrossRef](#)]
36. Lee, C.H.; Kang Thomas, H.K.; Kim, J.W.; Song, J.-K.; Kim, S. Seismic Performance of Concrete-Filled Tube Column-Reinforced Concrete Slab Connections with Shear Reinforcement. *ACI Struct. J.* **2019**, *116*, 233–244. [[CrossRef](#)]
37. Amini, A.B.; Palangsaraee, S.M. Effect of Rebar on Ductility of Moment-resisting Frame with Concrete-filled Tube Column. *Open Civ. Eng. J.* **2019**, *13*, 172–181. [[CrossRef](#)]
38. Park, Y.M.; Hwang, W.S.; Yoon, T.Y.; Hwang, M.-O. A new base plate system using deformed reinforcing bars for concrete filled tubular column. *Steel Compos. Struct.* **2005**, *5*, 375–394. [[CrossRef](#)]
39. Wang, H.J.; Lu, C.C.; Wei, H. Seismic analysis for concrete filled steel tube column row shear wall with steel plate energy dissipation bond. *J. Shenyang Univ. Technol.* **2016**, *38*, 228–234. [[CrossRef](#)]
40. Han, L.H.; Zhong, T.; Liu, W. Concrete filled steel tubular structures from theory to practice. *J. Fuzhou Univ. (Nat. Sci. Ed.)* **2001**, *29*, 24–34. [[CrossRef](#)]
41. Smoljanović, H.; Balić, I.; Munjiza, A.; Hristovski, V. Rotation-Free Based Numerical Model for Nonlinear Analysis of Thin Shells. *Buildings* **2021**, *11*, 657. [[CrossRef](#)]
42. Wang, Z.S.; Li, Y.K.; Wei, J.; Li, Q.; Shen, M.P. Hysteretic behavior and numerical analysis of thin-walled concrete-encapsulated steel tubular composite column with spiral ribs. *Chin. J. Appl. Mech.* **2021**, *38*, 2298–2305. [[CrossRef](#)]